Acta Crystallographica Section A
Foundations of Crystallography
ISSN 0108-7673

Received 7 September 2011
Accepted 26 October 2011

X-ray diffraction from nonperiodic layered structures with correlations: analytical calculation and experiment on mixed Aurivillius films

V. S. Kopp,[a]* V. M. Kaganer,[a] J. Schwarzkopf,[b] F. Waidick,[b] T. Remmele,[b] A. Kwasniewski[b] and M. Schmidbauer[b]

[a]Paul-Drude-Institute for Solid State Electronics, Berlin, Germany, and [b]Leibniz-Institute for Crystal Growth, Berlin, Germany. Correspondence e-mail: victor.kopp@pdi-berlin.de

X-ray diffraction from films consisting of layers with different thicknesses, structures and chemical contents is analysed. The disorder is described by probabilities for different sequences of layers. Closed analytical expressions for the diffracted X-ray intensity are obtained when the layers form a stationary Markov chain. The proposed model is applied to the diffraction data from epitaxial sodium bismuth titanate thin films with Aurivillius structure possessing such one-dimensional disorder. In this case, the disorder is caused by a random stacking of three and four perovskite units separated by bismuth oxide interlayers. The results of analytical calculations are in good agreement with the experimental data and indicate that the incorporation of sodium in the $Bi_4Ti_3O_{12}$ phase causes the formation of a fourth perovskite unit.

1. Introduction

X-ray diffraction is a primary tool to reveal periodicity in atomic arrangements. However, in real crystals the ideal periodicity is disturbed by various structural defects, *e.g.* point defects, dislocations, stacking faults, deviations from exact stoichiometry, surface and interfacial roughness, *etc*. For some defects (*e.g.* point defects, roughness), the average lattice is preserved and sharp Bragg peaks persist, accompanied by diffuse intensity in their vicinity. The problem appears to be more complicated when the disorder does not preserve the average lattice. For example, layer structures with layers of different thicknesses provide such a type of disorder. Here the position of a layer is determined by the sum of the thicknesses of all preceding layers, and the sequence of atomic layers is aperiodic. In many cases, this disorder can be described in terms of the probabilities of different layer sequences and more complicated diffraction patterns show up which cannot be easily interpreted without an appropriate simulation of X-ray diffraction.

The X-ray diffraction studies of one-dimensional disorder have a long history. Landau (1937) and Lifschitz (1937) first considered this problem theoretically. Their ideas were further developed in the works of Hendricks & Teller (1942), Kakinoki & Komura (1965), Kakinoki (1967), Welberry (1985), Seul & Torney (1989), Holstein (1993) and others. Kakinoki & Komura (1965) and Kakinoki (1967) developed a general description in terms of transfer matrices. Subsequently, using a generating function formalism, Seul & Torney (1989) derived the X-ray scattering function for a binary mixture with pure displacement disorder and nearest-neighbour correlations.

A very similar problem arises in the diffraction from stepped surfaces. The contribution of a terrace to the diffraction signal depends on the terrace location, which in turn depends on the positions and heights of all preceding steps. This problem was treated by Lent & Cohen (1984) and Pukite *et al.* (1985) who described diffraction profiles from stepped surfaces, with steps whose random distribution can be interpreted as a stationary Markov chain. Their approach was developed further by Croset & de Beauvais (1997, 1998) who proposed a clear and mathematically elegant description of the problem.

In this work, we have studied sodium bismuth titanate epitaxial films. These systems show a pronounced one-dimensional layer disorder in that different elementary unit cells with varying vertical dimensions are stacked. In order to simulate the experimentally observed X-ray diffraction profiles from these systems, we use the model based on the formalism of Croset & de Beauvais (1997, 1998) which was reformulated in order to correctly describe the observed one-dimensional layer disorder.

A statistical model of X-ray scattering by randomly disordered layers in application to complicated oxide structures, similar to ones considered in the present work, was developed by Holstein (1993). His study was restricted, however, to a completely random layer stacking without including correlations between neighbouring layers. In contrast, our model includes such correlations and Holstein's model is recovered as a limiting case.

We first describe in §2 the structure and growth of sodium bismuth titanate epitaxial films. §3 outlines the experimental setup for structural characterization of our oxide epitaxial

films. Then, in §4 the theory for the description of X-ray scattering from one-dimensional layer disorder follows in detail. Finally, in §5 the results of experiments and theory are compared and discussed.

2. Sodium bismuth titanate thin films

Sodium bismuth titanate based compounds are lead-free, ferroelectric materials with promising functional properties (Sanson & Whatmore, 2002; Park *et al.*, 1999; Bousquet *et al.*, 2010) showing Aurivillius or perovskite structure. Aurivillius phases consist of repeated layering of m perovskite units $(Bi_{m-1}Ti_mO_{3m-1})^{2-}$ (where some of the Bi atoms can be replaced by Na) alternating with bismuth oxide $(Bi_2O_2)^{2+}$ intermediate layers along the c axis. Starting from $Bi_4Ti_3O_{12}$ (an Aurivillius structure with m = 3), a series of layer-structured compounds with the general compositional formula $Bi_4Ti_3O_{12} + xNa_{0.5}Bi_{0.5}TiO_3$ have been derived: $Na_{0.5}Bi_{8.5}Ti_7O_{27}$ (m = 3.5), $Na_{0.5}Bi_{4.5}Ti_4O_{15}$ (m = 4) and $Na_{0.5}Bi_{0.5}TiO_3$ ($m = \infty$) (Sanson & Whatmore, 2005; Schwarzkopf *et al.*, 2011). $m = \infty$ indicates the absence of any $(Bi_2O_2)^{2+}$ layer, that means the pure perovskite structure, and m = 3.5 describes the interleaved structure made of alternate phases with m = 3 and m = 4. So far, only compounds with integer or half integer number m have been found. Generally, fractional m values correspond to mixed-layer structures, which contain perovskite-like slabs of different thicknesses.

Until now research on the material system $Bi_4Ti_3O_{12} + xNa_{0.5}Bi_{0.5}TiO_3$ has been essentially confined to the growth of bulk crystals and ceramics (Sanson & Whatmore, 2002; Uchida & Kikuchi, 1978; Ge *et al.*, 2008), while only a few authors have reported the deposition of thin films with $Na_{0.5}Bi_{0.5}TiO_3$ and $Na_{0.5}Bi_{4.5}Ti_4O_{15}$ structure (Bousquet *et al.*, 2010; Remondiere *et al.*, 2008; Zhou *et al.*, 2004). $Na_{0.5}Bi_{8.5}Ti_7O_{27}$ (m = 3.5) has not been grown in thin-film form so far. In this work, we report on sodium bismuth titanate thin films grown by metal–organic chemical vapour phase deposition (MOCVD).

The positions of the Bragg peaks in high-resolution X-ray diffraction patterns in combination with energy-dispersive X-ray spectroscopy have been used to successfully identify the sodium bismuth titanate phases with integer number m = 3 and m = 4 (Schwarzkopf *et al.*, 2011). However, for films deposited with a low Na/Bi ratio or at low substrate temperatures pronounced diffraction peak splittings and shifts are observed (Schwarzkopf *et al.*, 2011) which cannot be explained by the known structures $Bi_4Ti_3O_{12}$ (m = 3), $Na_{0.5}Bi_{8.5}Ti_7O_{27}$ (m = 3.5) or $Na_{0.5}Bi_{4.5}Ti_4O_{15}$ (m = 4). Zurbuchen *et al.* (2007) speculated that a peak splitting of the (008) Bragg peak may be caused by constructive interferences due to discrete local shifts in the magnitude of the apparent film layering repeat distance. In the present work, we demonstrate that the diffraction peak splittings and shifts are a direct consequence of a one-dimensional layer disorder which can be described as a stationary Markov chain.

3. Experimental

Sodium bismuth titanate films were deposited by liquid-delivery spin MOCVD. $Bi(thd)_3$ (thd = 2,2,6,6-tetramethyl-3,5-heptanedione), $Ti(O^iPr)_2(thd)_3$ (O^iPr = iso-propoxide) and Na(thd), dissolved in toluene, were used as source materials for Bi, Ti and Na, respectively. The films were deposited in an Ar/O_2 atmosphere with 38% O_2 at a constant pressure of 2.6×10^3 Pa. Different crystallographic sodium bismuth titanate phases were achieved by varying the substrate temperature between 873 and 1073 K, and the Na-to-Bi ratio in the source solutions between 0 and 3. In this way epitaxial thin films consisting of the Aurivillius phases $Bi_4Ti_3O_{12}$, which exclusively contain m = 3 blocks ($Bi_2Ti_3O_{10}$) between two $(Bi_2O_2)^{2+}$ intermediate layers, or $Na_{0.5}Bi_{4.5}Ti_4O_{15}$ with only m = 4 blocks ($Na_{0.5}Bi_{2.5}Ti_4O_{13}$) were obtained. Also several interleaved structures consisting of an alternate stacking of m = 3 and m = 4 blocks could be grown. All sodium bismuth titanate films were deposited on $SrTiO_3$(001) and $NdGaO_3$(110) substrates. Details of the deposition process have been described elsewhere (Schwarzkopf *et al.*, 2011).

The films exhibit thicknesses between 30 and 130 nm. They were characterized by high-resolution X-ray diffraction (HRXRD). A two-bounce Ge 220 channel-cut crystal monochromator was utilized to select the Cu $K\alpha_1$ line at λ = 1.5406 Å and to collimate the incident X-ray beam to 11 arcsec. Primary slits were used to define the beam size at the sample to about 0.3 × 5 mm, and corresponding slits were used in front of the detector. Strain-sensitive $\theta/2\theta$ scans were performed to record the scattered X-ray intensity distribution along the growth direction.

High-resolution transmission electron microscopy (HRTEM) was applied to investigate the film structure in more detail. Cross-section TEM samples were prepared by grinding on diamond lapping films and final argon ion milling with low-voltage ion sources using acceleration voltages from 4 kV down to 100 V and liquid-nitrogen cooling for the sample. The TEM investigations were performed with an FEI Titan 80–300 microscope equipped with an image C_S corrector and it was operated at 300 kV. The corrector was tuned to low C_S values and minimized residual aberrations to ensure a spatial resolution close to the limit of the instrument of about 0.07 nm.

For films exclusively composed of $Bi_4Ti_3O_{12}$ and $Na_{0.5}Bi_{4.5}Ti_4O_{15}$ exactly three or four perovskite blocks between two intermediate $(Bi_2O_2)^{2+}$ layers are seen on the HRTEM images (not shown here), respectively. Figs. 1(*a*) and 1(*b*) show the atomic and schematic structures of such three- and four-unit blocks. The A and B units are defined as consisting of three and four perovskite units, respectively, and one $(Bi_2O_2)^{2+}$ interlayer. The lengths of the A and B units correspond to half the c lattice parameter of $Bi_4Ti_3O_{12}$ and $Na_{0.5}Bi_{4.5}Ti_4O_{15}$, respectively.

Beside the 'pure' m = 3 and m = 4 phases, thin films with mixed phases could be observed. As an example Fig. 1(*c*) shows a cross-sectional HRTEM image of a sodium bismuth titanate layer stack with an irregular arrangement of A and B

units. In the following section we treat this irregular stacking in the framework of a one-dimensional Markov chain and develop a theory describing the X-ray scattering from such a one-dimensional stacking.

4. Theory

4.1. Diffracted intensity from a layered structure

Consider a sequence of N layers (Fig. 2). The layers have different thicknesses L_n and structure factors F_n. The bottom of the nth layer z_n is given by a sum of thicknesses of all preceding layers,

$$z_n = \sum_{k=1}^{n-1} L_k + z_0. \quad (1)$$

In the kinematic approximation, the diffraction amplitude for a given configuration of N consecutive layers is given by

$$A(Q) = \sum_{n=1}^{N} F_n(Q) \exp(iQz_n), \quad (2)$$

where $Q = 4\pi \sin\theta/\lambda$ is the scattering vector, 2θ being the angle between the incident and the diffracted waves, and λ is the X-ray wavelength. The diffracted intensity is the squared modulus of the amplitude,

$$\left|A(Q)\right|^2 = \sum_{n=1}^{N} \sum_{n'=1}^{N} F_n^*(Q) F_{n'}(Q) \exp\left[iQ(z_{n'} - z_n)\right], \quad (3)$$

where the asterisk denotes the complex conjugate. For further consideration, it is convenient to rewrite equation (3) in an equivalent form:

$$\begin{aligned} |A(Q)|^2 = &\sum_{n=1}^{N-1} \sum_{n'=n+1}^{N} F_n^* F_{n'} \exp[iQ(z_{n'} - z_n)] \\ &+ \sum_{n=1}^{N-1} \sum_{n'=n+1}^{N} F_n F_{n'}^* \exp[-iq(z_{n'} - z_n)] \\ &+ \sum_{n=1}^{N-1} F_n^* F_n. \end{aligned} \quad (4)$$

Let us denote

$$Y_{n,n'} = F_n^* F_{n'} \exp[iQ(z_{n'} - z_n)]. \quad (5)$$

Then, equation (4) can be written as

$$\left|A(Q)\right|^2 = \sum_{n=1}^{N-1} \sum_{n'=n+1}^{N} \left(Y_{n',n} + Y_{n',n}^*\right) + \sum_{n=1}^{N-1} Y_{n,n}. \quad (6)$$

The X-ray beam illuminates a large area of the sample that contains domains with different sequences of layers. Thus, the intensity [equation (6)] needs to be averaged over all possible realizations of the layer stacks. This is described in the next subsection.

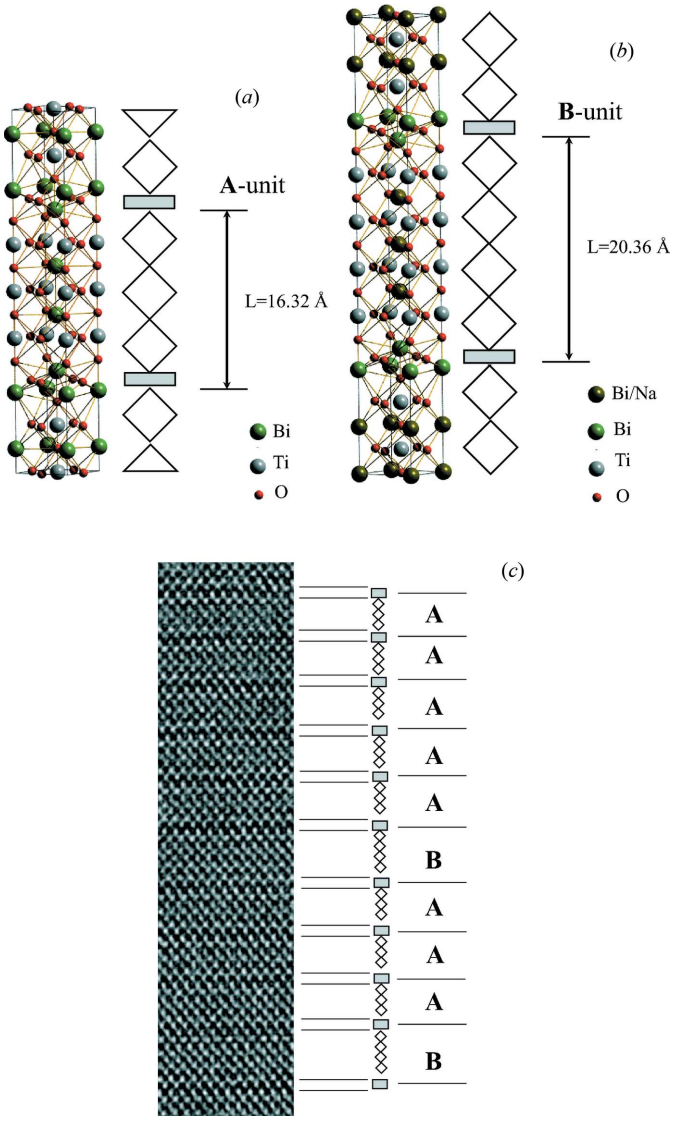

Figure 1
Atomic structure and schematics of Aurivillius phases with (*a*) three (m = 3, $Bi_4Ti_3O_{12}$) and (*b*) four perovskite units (m = 4, $Na_{0.5}Bi_{4.5}Ti_4O_{15}$) between two $(Bi_2O_2)^{2+}$ interlayers. The three- and four-unit blocks are denoted further on as *A* and *B* units. In the schematic representation, the rhomb symbolizes a perovskite unit and a grey rectangle the $(Bi_2O_2)^{2+}$interlayer. (*c*) Cross-sectional HRTEM image of a layer stack which contains both three and four perovskite units.

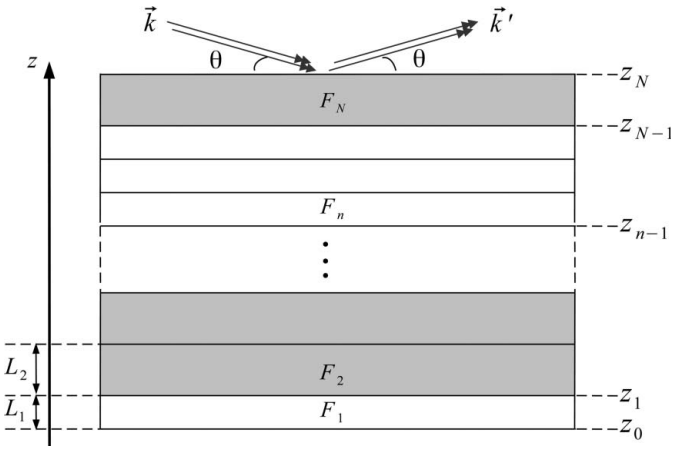

Figure 2
A schematic representation of a film with one-dimensional layer disorder.

4.2. Markov chains and average intensity

The nth layer can be in one of several states s_n characterized by the thickness L_{s_n} and the structure factor F_{s_n}. Fig. 1(*c*) shows an example of a film with monolayers in just two states, A and B (n = 1, 2). Further experimental examples presented in §5 demonstrate that two states are enough to model rather complicated layer distributions. Nevertheless, the analysis of the present section is quite general and allows an arbitrary number of states.

Let us denote by $P(s_{n'}, s_{n'-1}, \ldots s_n)$ the probability to observe the layers n', $n'-1, \ldots n$ in given states $s_{n'}$, $s_{n'-1}, \ldots s_n$. The average of a term [equation (5)] is

$$\langle Y_{n,n'} \rangle = \sum_{s_{n'}, \ldots s_n} P(s_{n'}, s_{n'-1}, \ldots s_n) Y_{n',n}. \tag{7}$$

In the following, we consider the states that constitute a stationary Markov chain with a finite number of states. That means the probability for the nth layer to be in a given state depends on the state of the previous layer only. We expect that this is a reasonable model for a crystal with layer disorder introduced during growth.

Denoting by $P(X|Y)$ the conditional probability of observing event X, provided Y is fixed, and using the well known formula for the conditional probability, we have

$$P(s_{n'}, s_{n'-1}, \ldots s_n) = P(s_{n'}|s_{n'-1}, \ldots s_n) P(s_{n'-1}, \ldots s_n). \tag{8}$$

For a Markov chain, the conditional probability in this equation is equal to $P(s_{n'}|s_{n'-1})$, since it depends only on the state of the preceding layer. It can be denoted as $P_{s_{n'}, s_{n'-1}}$. Then, equation (8) can be written as

$$P(s_{n'}, s_{n'-1}, \ldots s_n) = P_{s_{n'}, s_{n'-1}} P(s_{n'-1}, \ldots s_n), \tag{9}$$

and by recurrence,

$$P(s_{n'}, s_{n'-1}, \ldots s_n) = \prod_{k=n}^{n'-1} P_{s_{k+1}, s_k} \wp_{s_n}. \tag{10}$$

Here $\wp_{s_n}$ is the probability of finding the nth layer in the state s_n. For a stationary Markov chain, $\wp_{s_n}$ does not depend on n.

The relation [equation (1)] used in equation (5) provides

$$Y_{n,n'} = F_n^* F_{n'} \prod_{k=n}^{n'-1} \exp(iL_k Q). \tag{11}$$

Substituting the expressions for $Y_{n,n'}$ and $P(s_{n'}, s_{n'-1}, \ldots s_n)$ from equations (11) and (10), we have

$$\begin{aligned} \langle Y_{n,n'} \rangle = & \sum_{s_{n'}} F_{s_{n'}} \\ & \times \sum_{s_{n'-1}, \ldots s_{n+1}} \left[\prod_{k=n+1}^{n'-1} P_{s_{k+1} s_k} \exp(iQL_{s_k}) \right] \\ & \times \sum_{s_n} P_{s_{n+1} s_n} \wp_{s_n} F_{s_n}^* \exp(iQL_{s_n}). \end{aligned} \tag{12}$$

This equation can be written in a compact vector form, if we define the following vectors and matrices:

(*a*) vector $\vec{\wp}$ of stationary probabilities $\wp_s$,

(*b*) diagonal matrix $\hat{\wp}$ with elements equal to elements of stationary vector $\vec{\wp}$ (*i.e.* $\wp_{s's} = \delta_{s's} \wp_s$, where $\delta_{s's}$ is the Kronecker's symbol),

(*c*) vector $\vec{F}$ of structure factors F_s,

(*d*) matrix $\hat{P}$ of probabilities $P_{s's}$,

(*e*) matrix $\hat{T}$ of elements $T_{s's} = P_{s's} \exp(iQL_s)$. This matrix can be represented as a product $\hat{T} = \hat{P}\hat{E}$, where $\hat{P}$ is the probability matrix and $\hat{E}$ is the diagonal matrix with elements $E_{s's} = \delta_{s's} \exp(iQL_s)$,

(*f*) vector $\vec{W}$ of elements $W_s = \sum_{s'} P_{ss'} \exp(iQL_{s'}) \wp_{s'} F_{s'}^*$, or equivalently in the vector form $\vec{W} = \hat{P}\hat{E}\hat{\wp}\vec{F}^*$.

Then, equation (12) can be written as

$$\langle Y_{n,n'} \rangle = \vec{F}^T \hat{T}^{n'-n-1} \vec{W} \tag{13}$$

for $n \neq n'$ and

$$\langle Y_{n,n} \rangle = \vec{F}^T \hat{\wp} \vec{F}^* \tag{14}$$

for $n = n'$. Here $\vec{F}^T$ is the transposed vector. Now the summation of geometrical series in equation (6) can be performed, and finally we have

$$\left\langle |A(q)|^2 \right\rangle = 2\mathrm{Re}\left[N\vec{F}^T \hat{G} \vec{W} - \vec{F}^T \hat{G}^2 \left(\hat{I} - \hat{T}^N \right) \vec{W} \right] + N\vec{F}^T \hat{\wp} \vec{F}^*, \tag{15}$$

with $\hat{G} = \left(\hat{I} - \hat{T} \right)^{-1}$, where $\hat{I}$ stands for the identity matrix.

The inverse matrix $\hat{G}$ exists for all values of Q except some isolated values given by $\det\left(\hat{I} - \hat{T} \right) = 0$. The diffracted intensity at these points has to be calculated separately, taking into account that one of the eigenvalues of the matrix $\hat{T}$ becomes equal to 1, while other eigenvalues remain less than 1. The summation in equation (6) can be performed on the basis of the eigenvectors of the matrix $\hat{T}$, with separate summation for the eigenvalue 1 and all other eigenvalues. However, in the practical calculations below, we simply avoid calculating intensity at these special points and use equation (15).

4.3. Two-state system

Consider a system with two possible states, 1 and 2. The sequence of A and B layers in Fig. 2 is an example of such a system. We also consider below in §5 more complicated states, particularly the A layer as state 1 and the sequence AB as state 2. Therefore, we do not specify here the structures corresponding to states 1 and 2 and refer to A and B layers as a simplest realization of the two-state system.

Each state is uniquely characterized by its structure factor F_s (F_1 or F_2) and its length L_s (L_1 or L_2). The matrix $\hat{P}$ can be written as

$$\hat{P} = \begin{pmatrix} p & q \\ 1-p & 1-q \end{pmatrix}, \tag{16}$$

where p is the conditional probability of finding a layer in state 1 following the one in state 1 (an A unit follows an A unit in the simplest case). Analogously, $1-q$ is the conditional probability of finding a layer in state 2 following the one in state 2 (a B unit succeeds a B unit). The vector of stationary probabilities is given by

$$\vec{\wp} = (1 - p + q)^{-1} \begin{pmatrix} q \\ 1 - p \end{pmatrix}. \quad (17)$$

The parameters p and q control the consequent arrangement of the layers. Fig. 3 shows a schematic diagram of the $p - q$ plane, and denotes some specific statistical distributions of layers. For $p = 1$ and $1 - q = 0$ we find the system exclusively in state 1 (only A units, *i.e.* $Bi_4Ti_3O_{12}$ in the system $Bi_4Ti_3O_{12} + xNa_{0.5}Bi_{0.5}TiO_3$) while for $p = 0$ and $1 - q = 1$ we find the system exclusively in state 2 (only B units, *i.e.* $Na_{0.5}Bi_{4.5}Ti_4O_{15}$ for the same system). On the other hand, for $p = 0$ and $1 - q = 0$ we have alternating occupation of layers 1 and 2, *i.e.* the ideal $ABAB\ldots$ stacking (*i.e.* $Na_{0.5}Bi_{8.5}Ti_7O_{27}$).

Phase separation occurs for $p + (1 - q) > 1$, *i.e.* in the upper right triangle of Fig. 3. The diagonal $p = q$ connecting two pure phases is the locus of random stacking sequences. Along this line, the conditional probability of finding a layer in state 1 following the one in state 1 (or a layer in state 2 following the one in state 2) is equal to the stationary probability of finding a layer in state 1 (or 2), $p = q/(1 - p + q)$. This diagonal of the parametric diagram corresponds to the Holstein (1993) model.

Further, vectors and matrices defined above can be written as

$$\vec{F} = \begin{pmatrix} F_1 \\ F_2 \end{pmatrix},$$

$$\hat{T} = \begin{bmatrix} p\exp(iQL_1) & q\exp(iQL_2) \\ (1-p)\exp(iQL_1) & (1-q)\exp(iQL_2) \end{bmatrix},$$

$$\vec{W} = \begin{bmatrix} p\wp_1 F_1 \exp(iQL_1) + q\wp_2 F_2 \exp(iQL_2) \\ (1-p)\wp_1 F_1 \exp(iQL_1) + (1-q)\wp_2 F_2 \exp(iQL_2) \end{bmatrix}. \quad (18)$$

The average intensity is calculated analytically by substituting these expressions into equation (15).

5. Results and discussion

We first test and validate our model on the pure phases A and B (see Figs. 1*a*, 1*b*). The experimental $\theta/2\theta$ scans and corresponding calculated curves are shown in Fig. 4(*a*) (samples S1 and S4). The structure factors were calculated for the structures shown in Figs. 1(*a*), 1(*b*). For phase A ($Bi_4Ti_3O_{12}$) we use the data of Hervoches & Lightfoot (1999). The atomic coordinates of phase B ($Na_{0.5}Bi_{4.5}Ti_4O_{15}$) have been constructed accordingly using the coordinates of phase A with an extra perovskite unit. For phase B we have assumed that the sodium atoms replace Bi atoms with the probability 5%. Such replacement probability gives an appropriate intensity ratio of the diffraction peaks. The calculated curves are rather insensitive to the replacement probability: the use of 15% sodium in the calculation does not change the curves noticeably. The intensities have been normalized to the maximum intensity and the experimental background has been added to the simulated data in order to achieve a better matching.

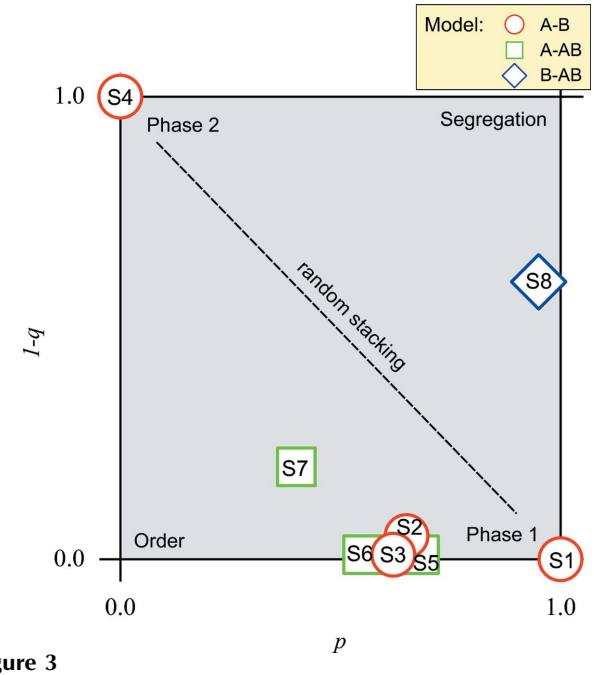

Figure 3
Parametric diagram of possible structures as a function of probabilities p and q. The values of the probabilities for the samples S1–S8 studied experimentally are shown. Different symbols correspond to different choices of the basic units.

The diffraction peak widths for the pure A and B phases are due to finite thicknesses of the epitaxial films. The truncation of the film gives rise to the thickness fringes in the calculated curves (see the curve S4 in Fig. 4*a*).

The average intensity [equation (15)] is obtained by summation of intensities scattered by different domains in the film. These domains contain, with given probabilities, different layer sequences. The number of layers in the stack N can also vary from one domain to the other, because of the film roughness. Croset & de Beauvais (1998) considered in detail the average over a broad distribution of the number of layers. In our case, the distribution is narrow and we perform calculations simply for fixed N values, which vary in different samples, depending on the film thicknesses, between 15 and 40. A choice of a certain N value from this range does not have any noticeable effect, except for the appearance of oscillations in the vicinity of the peaks at relatively small N. For example, for sample S4, N was fixed to 15, which results in oscillations in the simulation curve (see Fig. 4*a*).

The simulated peaks for the pure phases A and B (samples S1 and S4) are in good agreement with the experimental ones. For samples S2 and S3 in Fig. 4 the diffraction patterns are quite different compared to those of the pure phases: the original $Bi_4Ti_3O_{12}(004)$ peak is split into two peaks, while the $Bi_4Ti_3O_{12}(006)$ peak is shifted to higher 2θ values. The X-ray diffraction patterns consist of series of broad peaks that cannot be attributed as belonging to any periodic structure. However, the simulated X-ray profiles, obtained on the basis of an irregular stacking of A and B units, are in good agreement with the experimental ones: the peak locations and their intensities are in accordance with the experimental observa-

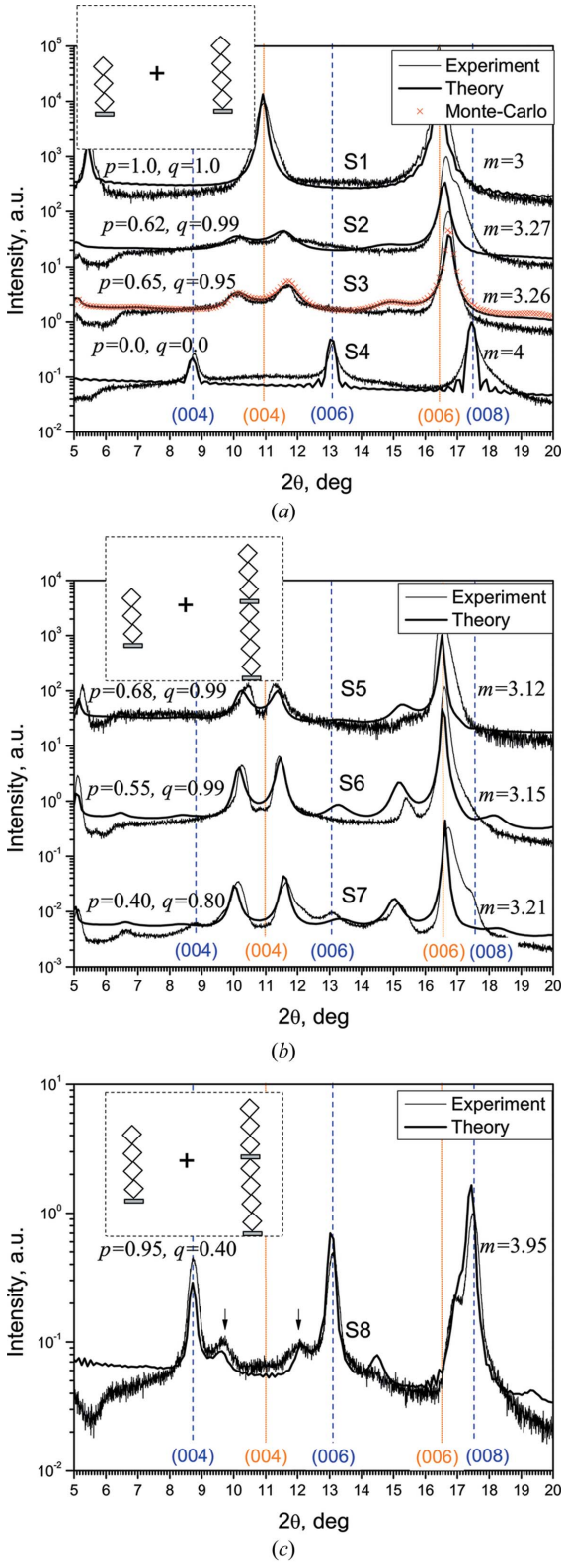

Figure 4
Experimental X-ray diffraction profiles and calculated curves for different choices of the basic units in the Markov chain: (*a*) *A*–*B*, (*b*) *A*–*AB*, (*c*) *B*–*AB* model. Arrows in (*c*) show the peak positions for the ordered *ABAB*... phase. The probabilities *p*, *q* and corresponding value *m* are indicated at each curve. The basic units used for the calculation are schematically shown in the insets. The diffraction peak positions for the pure *A* and *B* phases are marked by orange dotted lines and blue dashed lines, respectively.

tions. The probabilities p and q obtained from the fits are given in Fig. 4 and also shown in the parametric diagram of Fig. 3.

We have confirmed the analytical results by means of a Monte Carlo simulation. In the Monte Carlo calculation, a statistical ensemble of layer stacks is generated with the same probabilities as in the analytical calculation. The first layer at the interface is chosen to be in a state s with the probability equal to stationary probability $\wp_s$. A sum of intensities due to individual realizations of the layer stack is calculated. The results of the Monte Carlo calculations are shown in Fig. 4(*a*) for sample S3. The perfect coincidence of the X-ray profiles calculated analytically and by means of the Monte Carlo technique proves the correctness of the analytical results. In the following, we use throughout the analytical calculations for the analysis of the experimental profiles.

The experimental curves presented in Figs. 4(*b*), 4(*c*) cannot be fitted in the framework of the same model, *i.e.* as a Markov sequence of *A* and *B* layers. The origin of the disagreement is long-range-order correlations between non-adjacent layers. One might overcome this problem by including higher-order conditional probabilities, *i.e.* by proceeding from the Markov chains of rank 1 to chains of higher ranks. This approach, however, increases the size of the matrices and the number of parameters to be defined. We succeeded in describing the experimental curves in another way, by including more complicated layer sequences by means of redefinition of elementary units. A detailed HRTEM analysis, see Fig. 1(*c*), shows that in many samples the *B* layer is almost never followed by another *B* layer ($1 - q \simeq 0$). Then, we consider *A* and *AB* units as two possible elementary layers. This idea has proved to be quite productive. In Fig. 4(*b*), several experimental profiles are in good agreement with the calculated ones, obtained in the framework of the two-state theory of §4.3 but with the redefined elementary units as shown in the inset.

Fig. 4(*c*) presents an example of the experimental X-ray diffraction profile that needs another structural model. The strong peaks correspond to the pure phase of *B* layers, while additional weak peaks are in the middle between peak positions for pure *A* and *B* phases (marked by arrows in Fig. 4*c*) and therefore correspond to the ordered *ABAB*... layer sequence. We therefore model this diffraction profile by a sequence of *B* and *AB* units as the basic layers. Again, good agreement between experimental and calculated curves is obtained. The value $p = 0.95$ obtained by the fit points to long sequences of purely *B* units in the structure. That means that we can consider the film S8 as a superposition of separated phases of $m = 3.5$ and $m = 4$.

The parameters p and q obtained for samples S1–S8 are shown in the diagram of Fig. 3. Since they correspond to three different choices of basic units and cannot be directly compared, we use different symbols for each set of basic units.

For the interpretation of the experimental results one should remember that the substitution of Bi in the perovskite units by a Na ion is executed by the formation of a fourth perovskite unit between two adjacent $Bi_2O_2^{2+}$ layers in order to provide charge neutrality (Schwarzkopf *et al.*, 2011). That means that Na is incorporated in *B*-type layers only. From the

evaluated parameters p and q two main conclusions can be drawn.

First, for the physical interpretation of the parameters p and q we have to consider different deposition conditions of the films S1–S8. S1 was deposited at a low substrate temperature (923 K) without any Na in the gas phase and, consequently, results in a pure $Bi_4Ti_3O_{12}$ phase. When Na is introduced in the gas phase, the films consist of an irregular arrangement of three perovskite units (which do not contain any Na) and four perovskite units (which contain Na on Bi sites). The Na supply in the gas phase during the deposition process was sequentially increased from S2 to S3 to S4. Simultaneously the value p, which indicates the probability that a unit A follows a unit A, decreases (Fig. 3). That is to say that more and more B units were incorporated which is correlated with an increased Na incorporation in the films. A similar effect can be observed for increasing substrate temperature during the deposition process. S5, S6 and S7 were deposited at low Na concentration in the gas phase but increasing substrate temperature. Here, p decreases again, which is attributed to an enhanced incorporation of Na-containing B units. Higher temperature seems to promote the incorporation of Na ions on Bi sites. Sample S8 (high substrate temperature, low Na supply) shows a significant increase of the value p (for relatively high $1 - q$ value) which according to Fig. 3 might be interpreted as an increasing tendency for phase segregation. The reason for this behaviour is not yet clear.

Secondly, the comparison of the simulations with the experimental HRXRD patterns reveals that not only phases with an integer number m in the system $Bi_4Ti_3O_{12} + xNa_{0.5}Bi_{0.5}TiO_3$ like the pure $Bi_4Ti_3O_{12}$ (only A units) or the pure $Na_{0.5}Bi_{4.5}Ti_4O_{15}$ (only B units) develop during film growth, but rather fractional m numbers are also possible.

A fractional m can be determined through the parameters p and q. If we define the parameter m as the mean number of perovskite units between two $(Bi_2O_2)^{2+}$ interlayers, then using the stationary probability vector $\vec{\wp}$ we can write

$$m = \wp_1 m^{(1)} + \wp_2 m^{(2)}$$

$$= \frac{q m^{(1)} + (1-p) m^{(2)}}{1 - p + q}, \qquad (19)$$

where $m^{(i)}$ are the numbers of perovskite units between two $(Bi_2O_2)^{2+}$ interlayers in unit blocks used for simulation and the explicit expressions for $\wp_i$ from equation (17) were used.

The values of m calculated with the help of equation (19) are presented in Fig. 4. The calculated values are almost always in the range of $3 < m < 3.5$ (excluding films consisting of a pure A or a pure B phase). From these results and in agreement with the HRTEM observations, we conclude that the pure recurrent intergrowth of A and B units, which should lead to an ordered $m = 3.5$ structure ($ABAB\ldots$), was not realized under our preparation conditions. This observation is in contradiction to Mallick *et al.* (2005), who have reported the $Na_{0.5}Bi_{8.5}Ti_7O_{27}$ phase with $m = 3.5$ for bulk materials. We tentatively attribute the disordered arrangement of A and B units to the absence of elastic forces (due to equal in-plane parameters of the A and B units) or charge-ordering interactions between the A and B units in the $Bi_4Ti_3O_{12} + xNa_{0.5}Bi_{0.5}TiO_3$ system unlike Rao & Thomas (1985) for $Bi_9Ti_6CrO_{27}$ or Gopalakrishnan *et al.* (1984) for $Bi_5Nb_3O_{15}$.

6. Conclusions

We present a statistical model of X-ray scattering from partially disordered epitaxial films containing a finite number of layers of different structures and thicknesses. The analysis is made in terms of probabilities of different layer sequences. We find that a wide range of the X-ray diffraction profiles from sodium bismuth titanate films can be described as layer sequences with only nearest-neighbour correlations. Specifically, the disorder is well described by the model of stationary Markov chains with nearest-neighbour transition probabilities. Using the well developed theory of the Markovian processes, we have established fully analytical expressions for the intensity diffracted by disordered epitaxial films.

The simulations were performed for a variety of sodium bismuth titanate oxide films and are in good agreement with the experimental data. Together with HRTEM images they indicate that the incorporation of sodium in the $Bi_4Ti_3O_{12}$ phase causes the formation of a fourth perovskite unit. Beside the 'pure' ordered phases $Bi_4Ti_3O_{12}$ ($m = 3$, $p = 1$, $1 - q = 0$) and $Na_{0.5}Bi_{4.5}Ti_4O_{15}$ ($m = 4$, $p = 0$, $1 - q = 1$) we found disordered phases with fractional numbers m which lead to Bragg peak splitting and shifts in the X-ray diffraction curves. For almost all samples under consideration we found values for m between 3.0 and 3.5. In other words, the probability of finding two sequential layers consisting of four perovskite units is very low. The disorder is found to be strongly dependent on the conditions of film deposition. None of the investigated films has revealed a pure $m = 3.5$ structure, which is attributed to the absence of additional ordering forces. The presented method turns out to be suitable for describing disordered intergrowth systems.

VSK and VMK thank Karl Sabelfeld for fruitful discussions. The work was partially funded by Deutsche Forschungsgemeinschaft (DFG) grant No. KA 3262/2-1.

References

Bousquet, M., Duclere, J.-R., Champeaux, C., Boulle, A., Marchet, P., Catherinot, A., Wu, A., Vilarinho, P. M., Deputier, S., Guilloux-Viry, M., Crunteanu, A., Gautier, B., Albertini, D. & Bachelet, C. (2010). *J. Appl. Phys.* **107**, 034102.
Croset, B. & de Beauvais, C. (1997). *Surf. Sci.* **384**, 15–35.
Croset, B. & de Beauvais, C. (1998). *Surf. Sci.* **409**, 403–412.
Ge, W., Liu, H., Zhao, X., Zhong, W., Pan, X., He, T., Lin, D., Xu, H., Jiang, X. & Luo, H. (2008). *J. Alloys Compd*, **462**, 256–261.
Gopalakrishnan, J., Ramanan, A., Rao, C., Jefferson, D. & Smith, D. (1984). *J. Solid State Chem.* **55**, 101–105.
Hendricks, S. & Teller, E. (1942). *J. Chem. Phys.* **10**, 147–167.
Hervoches, C. H. & Lightfoot, P. (1999). *Chem. Mater.* **11**, 3359–3364.
Holstein, W. L. (1993). *J. Appl. Phys.* **74**, 4963–4971.
Kakinoki, J. (1967). *Acta Cryst.* **23**, 875–885.

Kakinoki, J. & Komura, Y. (1965). *Acta Cryst.* **19**, 137–147.
Landau, L. D. (1937). *Phys. Z. Sov. Union*, **12**, 579–585.
Lent, C. & Cohen, P. (1984). *Surf. Sci.* **139**, 121–154.
Lifschitz, I. (1937). *Phys. Z. Sov. Union*, **12**, 623–643.
Mallick, S., Bowman, K. & King, A. (2005). *Appl. Phys. Lett.* **86**, 182802.
Park, B. H., Kang, B. S., Bu, S., Noh, T., Lee, J. & Jo, W. (1999). *Nature* (*London*), **401**, 682–684.
Pukite, P., Lent, C. & Cohen, P. (1985). *Surf. Sci.* **161**, 39–68.
Rao, C. & Thomas, J. (1985). *Acc. Chem. Res.* **18**, 113–119.
Remondiere, F., Malic, B., Kosec, M. & Mercurio, J.-P. (2008). *J. Sol-Gel Sci. Technol.* **46**, 117–125.
Sanson, A. & Whatmore, R. W. (2002). *Jpn. J. Appl. Phys.* **41**, 7127–7130.
Sanson, A. & Whatmore, R. W. (2005). *J. Am. Ceram. Soc.* **88**, 3147–3153.
Schwarzkopf, J., Schmidbauer, M., Duk, A., Kwasniewski, A., Anooz, S. B., Wagner, G., Devi, A. & Fornari, R. (2011). *Thin Solid Films*, **520**, 239–244.
Seul, M. & Torney, D. C. (1989). *Acta Cryst.* A**45**, 381–396.
Uchida, K. & Kikuchi, T. (1978). *J. Am. Ceram. Soc.* **61**, 5–8.
Welberry, T. (1985). *Rep. Prog. Phys.* **48**, 1543–1593.
Zhou, Z. H., Xue, J. M., Li, W. Z., Wang, J., Zhu, H. & Miao, J. M. (2004). *Appl. Phys. Lett.* **85**, 804–806.
Zurbuchen, M., Tian, W., Pan, X., Fong, D., Streiffer, S., Hawley, M., Lettieri, J., Jia, Y., Asayama, G., Fulk, S., Comstoc, D., Knapp, S., Carim, A. & Schlom, D. (2007). *J. Mater. Res.* **22**, 1439–1471.